Piezoelectric Quantum 1/f Noise in Nitride-Based Heterostructures

Peter H. Handel[a], Hadis Morkoc[b], Engkee Sia and Amanda M. Truong[a]
[a]Department of Physics & Astronomy and Center for Nanoscience, Univ. of Missouri, St. Louis, MO 63121, USA
[b]Virginia Commonwealth University, ECE Department, Richmond, VA 23284

There are as many types of quantum 1/f noise [1], [2], as there are systems of massless infraquanta with infrared-divergent coupling to the current carriers. Each of these types has a conventional and coherent part, corresponding to terms in the hamiltonian that are proportional with the first and second power of the number of carriers defining the current, respectively. In piezoelectric materials, particularly those also showing ferroelectric spontaneous polarization, transversal phonons are the massless quanta leading to piezoelectric, or lattice-dynamic, quantum 1/f effects, again both conventional and coherent. As in the usual QED case, the observable 1/f noise is approximated by a weighted sum of the conventional and coherent quantum 1/f effects. The sum involves the coherence parameter, this time denoted by s', in the weight factors. The parameter s' is also estimated from first principles. The general formula involving s' is applied to bulk GaN and AlGaN grown with different methods, and includes the dependence on stress and polarization. It also includes the dependence on stress and the geometry of the sample. It is important both for reliability testing and for general device optimization.

Keywords: Quantum 1/f noise, GaN, AlGaN, Ferroelectric Nitride compound semiconductors, Conventional quantum 1/f effect, 1/f noise in Heterostructures, Noise in HFETs and MODFETs, 1/f noise-based FET reliability tests.

1. INTRODUCTION

The best known form of quantum 1/f noise [1]-[2] is certainly the electromagnetic, or QED form, that has been used to improve semiconductor devices other than the MOSFET and many other high-tech devices, sensors, and systems since the 1980s. Both the coherent and conventional QED-type Quantum 1/f Effect (Q1/fE) contribute to quantum 1/f noise, and are caused by the infrared divergent coupling between charged particles and soft photons. In final analysis, this new aspect of quantum mechanics is therefore due to the non-linearity of the system of particle and field, where the field reacts on the particles that generated the field in the first place.

The conventional Q1/fE is a new property of the "physical cross sections and process rates" introduced by one of us in order to allow quantum mechanics to explain fundamental 1/f noise in materials, devices and systems, including phase noise. It does not depend on the presence of other similar charged particles drifting in the electrical field.

The coherent Q1/fE, on the other hand, is a basic property of any particle. It is caused by the uncertainty of its rest mass, due to the same infrared divergent coupling and due to the coherent state in which the photon states happen to be. This coherent state of the field is simply due to the presence of the particles and due to their motion.

The energy of coherent states is uncertain, as is known since Schrödinger introduced them in the 1920s. This uncertainty, derived from Heisenberg's uncertainty principle, causes the state of any particle to be non-stationary and beset by the fundamental coherent quantum 1/f noise $2\alpha/\pi f$, where $\alpha=e^2/\hbar c=1/137$ is Sommerfeld's fine structure constant. It is remarkable that the power spectral density of fractional fluctuations $2\alpha/\pi f$ in current, votage, mobility, diffusion constant, recombination speed, quartz resonator dissipation rate and frequency, etc., etc, contains Planck's constant in the denominator.

That makes this new aspect of quantum mechanics, or most important and fundamental form of quantum chaos, particularly interesting. It is the one that shapes our very existence, and causes us to like spontaneously, for instance, 1/f, or symphonic, music. Epistemologically, quantum 1/f noise is just a special case of the fundamental universal 1/f spectrum, caused by the simultaneous presence of nonlinearity and a special form of homogeneity in any system, e.g., traffic on the highways. This is described by Handel's "Sufficient Criterion," that is satisfied also by QED at low frequencies.

The drift motion of the current carriers, mentioned in the previous paragraph, causes a magnetic field and a magnetic form of kinetic energy, $LI^2/2$ where L is the inductance. In a thick copper wire, it is much larger than the mechanical form of the kinetic energy of the same drift motion of the current carriers. This magnetic energy of the drift motion of an

electron is proportional to the number of other electrons, per unit length of the wire, that are drifting along with drift velocity v that is their average velocity. On the other extreme of a nanoscopically thin semiconductor, the mechanical form $mv^2/2$ dominates, as was pointed out already at the start of the theory of fundamental 1/f noise. Therefore we understand why the coherent Q1/fE is found to be dominant in a copper wire, while the conventional Q1/fE is found to be dominant in the very thin, poorly doped semiconductor whisker.

In Sec. 2 below we review the elementary relation between coherent and conventional Q1/fE [3] that is suggested by the relation between the magnetic and kinetic drift energies for the electromagnetic or quantum electrodynamical (QED) case, in which photons are the infraparticles. In Sec. 2 we repeat this more formally. In Sec. 3 we extend this treatment to the case of piezoelectric quantum 1/f noise, in which soft (transversal) piezophonons are the infraparticles. This was also introduced as Quantum Lattice-Dynamical (QLD) quantum 1/f noise. There is one type of quantum 1/f noise for each system of infraquanta with infrared divergent coupling to the current carriers, as Handel pointed out already in his review article at the First International Conference on 1/f Noise in Tokyo, in 1977. Each of these types of quantum 1/f noise, comprise a coherent Q1/fE and a conventional Q1/fE.

The application to QLD allows us for the first time to explain the giant quantum 1/f noise in large ferroelectric semiconductor samples of BaSrTiO3, GaN and AlGaN. The speed of sound replaces the speed of light in the denominator of α, and the observed 1/f noise is 10^6 times larger, as expected from the theory. But there are no low frequency piezophonons, even in the largest semiconductor samples. In Sec. 4 we show that a system of subharmonics generates a similar hierarchy of states as the harmonics can generate. This is intimately related to the realization that nonlinearity causes all fundamental 1/f noise, of any nature.

2. ELEMENTARY DERIVATION OF THE PARAMETER s'

We suggest that the relation of the coherent Q1/fE to the conventional Q1/fE is described in a first, rough, approximation through the parameter s defined here. The coherent state in a conductor or semiconductor sample is the result of the experimental efforts directed towards establishing a steady and constant current. It is, therefore, the state defined by the collective motion, i.e. by the drift of the current carriers. It is expressed in the hamiltonian by the magnetic energy E_m, per unit length, of the current carried by the sample. In very small samples or electronic devices, this coherent magnetic energy

$$E_m = \int(B^2/8\pi)d^3x = [nevS/c]^2\ln(R/r) \tag{1}$$

is much smaller than the total kinetic energy E_k of the drift motion of the individual carriers

$$E_k = \sum mv^2/2 = nSmv^2/2 = E_m/s. \tag{2}$$

Here we have introduced the magnetic field B, the carrier concentration n, the cross sectional area S and radius r of the cylindrical sample (e.g., a current carrying wire), the radius R of the electric circuit, and the "coherence ratio"

$$s = E_m/E_k = 2ne^2S/mc^2\ln(R/r) \approx 2e^2N'/mc^2, = 2N'r_o. \tag{3}$$

Here $N' = nS$ is the number of carriers per unit length of the sample, $r_o = e^2/mc^2 = 2.8\cdot10^{-13}$ cm is known as the classical radius of the electron, and the natural logarithm ln(R/r) has been approximated by one in the last form. We expect the total observed spectral density of the mobility fluctuations to be given by a relation of the form

$$(1/\mu^2)S_\mu(f) = [1/(1+s)][2\alpha A/fN] + [s/(1+s)][2\alpha/\pi fN] = [2\alpha/(1+s)fN][A+s/\pi], \tag{4}$$

which can be interpreted as an expression of the effective Hooge constant if the number N of carriers in the (homogeneous) sample is brought to the numerator of the left hand side. In this equation $\alpha A = 2\alpha(\Delta v/c)^2/3\pi$ is the usual nonrelativistic expression of the infrared exponent, present in the familiar form of the conventional quantum 1/f effect. This equation is limited to quantum 1/f mobility (or diffusion) fluctuations, and does not include the quantum 1/f noise in the surface and bulk recombination cross sections in the surface and bulk trapping centers, in tunneling and injection processes, in emission or in transitions between two solids.

Note that the coherence ratio s introduced here equals the unity for the critical value $N' = N'' = 2\cdot10^{12}$/cm., e.g. for a cross section $S = 2\cdot10^{-4}$ cm^2 of the sample when $n = 10^{16}$. For small samples with $N' \ll N''$ only the first term survives, while for $N' > N''$ the second term in Eq. (4) is dominant. In practice, s is therefore twice the number of carriers in a salami slice perpendicular to the direction of the current, with a thickness given by the classical radius of the electron.

3. QED DERIVATION OF THE PARAMETER s

In QED, the displacement amplitude of the electromagnetic oscillator with wave vector q and polarization ε is the Fourier component of the vector potential expanded over a cubic box of volume V

$$Z_q = \frac{ek^\mu \varepsilon_\mu}{\vec{k}\cdot\vec{q} - m\omega_q/\hbar}\cdot\frac{1}{\sqrt{2\hbar cqV}} \approx \frac{ek^\mu \varepsilon_\mu}{-mc}\cdot\frac{\hbar}{\sqrt{2\hbar cq^3 V}} \tag{5}$$

It is produced by the presence of an electron of wave vector k, charge e and mass m. It is well known that the electron moving with velocity **v** generates a vector potential

$$\boldsymbol{A} = \frac{e\vec{v}}{4\pi cr} = \frac{\vec{v}}{c}\Phi \Longrightarrow \xrightarrow{Fourier} \frac{e\vec{v}}{cq^2} = \frac{e\hbar\vec{k}}{mcq^2} \tag{6}$$

On the right we have shown the Fourier transform, and Φ is the electric potential. This coincides with Eq. (5), if we apply the normalization for Fourier expansion in a box of volume V. The current density of the electron is

$$\vec{j} = e\vec{v}\,\delta(\vec{r}) \xrightarrow{Fourier} e\vec{v} \tag{7}$$

The motional part of the energy is

$$W_{motion} = \tfrac{1}{2}\int \frac{\vec{j}}{c}\cdot\vec{A}\,d^3r = \tfrac{1}{2}\frac{\vec{j}}{c} * \vec{A} = \tfrac{1}{2}\int e\vec{v}\,\frac{e\vec{v}}{cq^2}4\pi\frac{dq}{(2\pi)^3} = \frac{e^2v^2}{4\pi^2c^2}q_{\max} = \frac{e^2v^2}{4\pi^2c^2}\frac{\pi}{2r_0} \tag{8}$$

Here * indicates a convolution and r_o is the classical radius of the electron, introduced in the previous section. The upper cutoff q_{max} introduced here for q, corresponds to a lower cutoff r_o for the first integral in Eq. (8). By carrying out that first integral we get

$$W_{motion} = \frac{e^2v^2}{8\pi r_0' c^2} \tag{9}$$

and by comparing with the q-space integral, we obtain

$$q_{max} = \pi/2r_o. \tag{10}$$

We now have all the ingredients for a discussion of the piezoelectric, i.e., Quantum Lattice-Dynamic Quantum 1/f Effect case.

4. CONNECTION OF COHERENT AND CONVENTIONAL QLD-Q1/fE

The conventional, or incoherent, piezoelectric quantum 1/*f* noise effect [3]-[5] is given for small samples or devices by

$$\frac{S_\sigma(f)}{\langle\sigma\rangle^2} = \frac{2gA}{fN} \tag{11}$$

with $A = 2(\Delta v)^2/3\pi(v_s)^2$, Δv is the change of electron velocity during scattering and σ is any scattering cross section defined for carriers that exhibit piezoelectric coupling to ELF phonons. Here g is the dimensionless piezopolaron coupling constant, similar to the fine structure constant α, but with the speed of transversal sound waves replacing the speed of light in the denominator. It also involves a geometrical constant of the order of unity, dependent on the lattice. In a first approximation, σ can also be the mobility μ, the conductivity, or the current *j*. In the coherent case [4] of large devices,

$$\frac{S_j(f)}{j^2} = \frac{4g}{\pi f}\frac{1}{\left[1-\left(\hbar k_s/m^* v_s\right)^2\right]} \tag{12}$$

Here $|\mathbf{v}| = u$ is the drift velocity of the carriers, m* their effective mass, and v_s is the speed of sound for transversal acoustic phonons. In this section we derive the connection between the coherent and conventional forms of Lattice-Dynamical (piezoelectric) Quantum 1/f Effect (LD-Q1/fE) similarly to the way this was done in 1985 for the usual QED-Q1/fE [3].

In QLD, the amplitude of the piezo-elastic transversal lattice mode with wave vector q is the Fourier component q of the displacement caused by an electron in the lattice, expanded over a cubic box of volume V

$$A_{\vec{q}} = \frac{-iv_s(2\pi g / q^3 V)^{1/2}}{v_s - \hbar\hat{q}\cdot\vec{k}/m} \tag{13}$$

This is similar to Eq. (5). The part corresponding to the motion is obtained by subtracting the static part (Eq. 13 for k=0) that applies for an electron at rest

$$A_{\vec{q}}^{mot} = -iv_s\left(\frac{2\pi g}{q^3 V}\right)^{\frac{1}{2}}\left[\frac{1}{v_s - \hbar\hat{q}\cdot\vec{k}/m} - \frac{1}{v_s}\right] = -iv_s\left(\frac{2\pi g}{q^3 V}\right)^{\frac{1}{2}}\frac{\hbar\hat{q}\cdot\vec{k}}{mv_s(v_s - \hbar\hat{q}\cdot\vec{k}/m)} \tag{14}$$

The corresponding motional energy W^{mot} for an electron of wave vector k is thus

$$v_s^{-2}W_{\vec{k}}^{mot} = \sum_{\vec{q}} |A_{\vec{q}}^{mot}|^2 \hbar\omega_q = \frac{2\pi g}{V}\frac{\hbar^3}{m^2 v_s}\frac{V}{(2\pi)^3}\int d\Omega\int_0^{q_D} dq\,\frac{k^2\cos^2\theta}{(v_s - \hbar k\cos\theta/m)^2} \tag{15}$$

Here q_D is the Debye wave vector. The integration yields

$$W_{\vec{k}}^{mot} = \frac{g\hbar^3}{2\pi m^2 v_s}\frac{V}{(2\pi)^3}\int_0^{q_D} dq\int_{-1}^{1}\frac{k^2x^2dx}{(1-\hbar kx/mv_s)^2} = \frac{g}{2\pi}\frac{mv_s^2 q_D}{k}F(\frac{v}{v_s}) \tag{16}$$

With $q_D = 1/r'_0$, we obtain thus for cylindrical symmetry

$$W_{\vec{k}}^{mot} = \frac{g}{2\pi}\frac{mv_s^2}{kr'_o}F(\frac{v}{v_s}) \xrightarrow{Cylindrical-Symm} \frac{g}{2\pi}\frac{mv_s^2}{kr'_o}F(\frac{v}{v_s})N'\ln\frac{R}{r'_0} \tag{17}$$

N' is again the number of carriers per unit length of the sample in the direction of current flow, and *m** is the electron effective mass. Here we introduced the function

$$F(u/v_s) = 2(u/v_s)\{1 + 1/[1 - (u/v_s)^2]\} + \ln[1-(u/v_s)]^2 - \ln[1+(u/v_s)]^2. \tag{18}$$

We introduce the ratio of the coherent piezoelectric energy of the drift motion divided by the additional kinetic energy of the carriers introduced by the drift velocity u.

$$s' = \frac{\frac{g}{2\pi}\frac{mv_s^2}{kr'_o}F(\frac{u}{v_s})N'\ln\frac{R}{r'_0}}{N'mu^2/2} = \frac{g}{\pi}\frac{v_s^2}{u^2 kr'_o}F(\frac{u}{v_s})\ln\frac{R}{r'_0} \tag{19}$$

This is the desired ratio s' of terms present in the hamiltonian, corresponding in QLD to the parameter s.

As before, the coherent and conventional forms of QLD-Q1/fE are superposed with weights s/(1+s) and 1/(1+s). For the intermediate case, i.e., for sizes in between coherent and incoherent, we have $S_j(f)/j^2 = \alpha/Nf$ with α defined as

$$\alpha = \alpha_{incoh}\frac{1}{(1+s')} + \alpha_{coh}\frac{s'}{(1+s')} \tag{20}$$

Again, similar to s, the weight s' is the ratio between the piezoelectric or LD form of kinetic energy [associated with the electric current present in the sample or device, that is coherent], and the incoherent kinetic energy $m_{eff}u^2/2$ of individual particles, [caused by the drift velocity u].

The function F present in the definition of s' is given by Eq. (18) as

$$F(u/v_s) = 2(u/v_s)\{1+1/[1-(u/v_s)^2]\} + \ln[1-(u/v_s)]^2 - \ln[1+(u/v_s)]^2. \tag{21}$$

For $u/v_s << 1$, $F(u/v_s) = (2/3)(u/v_s)^3$; then *s*' can be simplified as $s' = 2gN'\hbar/3\pi m^* v_s$. This expression can be used for small drift velocity, much smaller than the sound velocity in the semiconductor. For $1-(u/v_s) << 1$, $F(u/v_s) = 1/[1-(u/v_s)]$, then *s*' can be approximated as $s' = (gN'\hbar/\pi m^* v_s)(v_s/u)^3\{1/[1-(u/v_s)]\}$, which is very large. This expression is used for drift velocities approaching the speed of sound.

5. EXPERIMENTAL TEMPERATURE-DEPENDENT RESISTIVITY

The resistivity of both ELO-GaN (epitaxial lateral overgrowth generated) and n^+-GaN:Si (doped) samples was measured for temperature varying from 100-550K. As illustrated in Fig. 5.1, it is revealed that resistivity decreases as temperature increases (100-300K) for both ELO-GaN and n^+-GaN:Si. This is attributed to the fact that ionized impurity scattering is dominating [6]. As the temperature increases further (300-530K), the resistivity for ELO-GaN decreases, but that for n^+-GaN:Si increases. The later phenomenon is attributed to crystal defect scattering [6]. Since the presence of a lattice defect is always associated with an increase of the electrical resistivity and the fact that the dislocation density of ELO-GaN is significantly lower compared to n^+-GaN:Si, hence the resistivity of ELO-GaN decreases with increasing temperature.

Fig. 5.1 also reveals that the change of the measured resitivity for ELO-GaN at high temperature (300–500K) is negative whereas for n^+-Ga:Si is positive. The resistance change is expressed as [7]

$$\frac{\Delta R}{R} = \frac{\Delta\rho}{\rho} + 4\gamma\frac{1-2\nu}{1-\nu}s|\Delta\varepsilon| = \frac{\Delta\rho}{\rho} + s\beta|\Delta\varepsilon| \tag{22}$$

where $\Delta\rho = \rho_D\Delta n_D$; Δn_D is the variation of dislocation density; ρ_D is the dislocation resistivity; γ is the Grüneisen's constant; ν is the Poisson ratio; $\Delta\varepsilon$ is the strain variation and $s = \pm 1$ according to whether the stress is compressive (s = +1) or tensile (s = -1). The total resistivity ρ contains vacancies, interstitials and dislocations with respective densities n_v, n_I and n_D. It is usually expressed as $\rho = \rho_{ph} + \rho_v n_v + \rho_I n_I + \rho_D n_D$ where ρ_{ph} represents the phonon contribution. The term $s\beta|\Delta\varepsilon|$ incorporates the piezoelectric resistance changes. Since the thermal expansion coefficients of GaN and Al_2O_3 are respectively $\alpha_{GaN} = 5.45\times10^{-6}$/°C and $\alpha_s = 7.5\times10^{-6}$/°C [8], and $\alpha_{GaN} < \alpha_s$, heating from the unstressed state leads to tension, cooling to compression. For GaN material, $\gamma = 1.8$ [9], therefore, the term incorporating the piezoelectric resistance changes $s\beta|\Delta\varepsilon|$ in (3.1) is negative since s is negative (tension) at high temperature. From Fig. 5.1, we can infer that $s\beta|\Delta\varepsilon| > \Delta\rho/\rho$ for ELO-GaN in Eq. (22) and the reverse is true for n^+-GaN:Si. This leads us to conclude that dislocation rearrangement (and other defects) dominates in n^+-GaN:Si whereas piezoelectric effect dominates for ELO-GaN at high temperature.

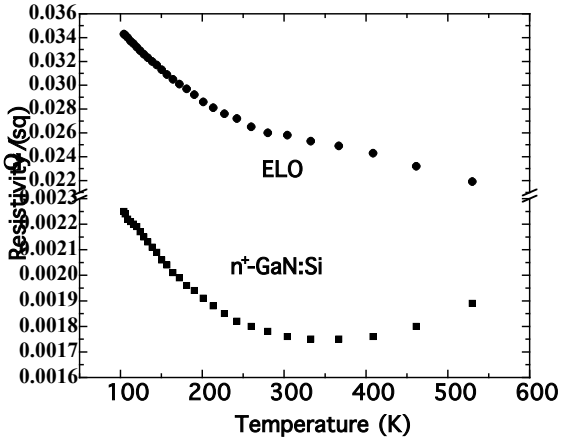

Fig. 5.1: Temperature-dependent resistivity of ELO-GaN and n^+-GaN:Si.

6. LOW FREQUENCY NOISE CHARACTERISTICS

6.1 Epitaxial Lateral Overgrown GaN

In evaluating the noise parameter α, the operating voltage range was selected to be less than 0.05V. The voltage power spectral densities S_V as well as S_V with error bars are shown in Fig. 3.6a and 3.6b, respectively, for ELO-GaN measured at 130K and 550K at a constant biasing current of 0.2mA. The spectra show $1/f$ behavior below 50Hz. The noise parameter can be estimated experimentally as $\alpha = S_I f N / V^2$ [10].

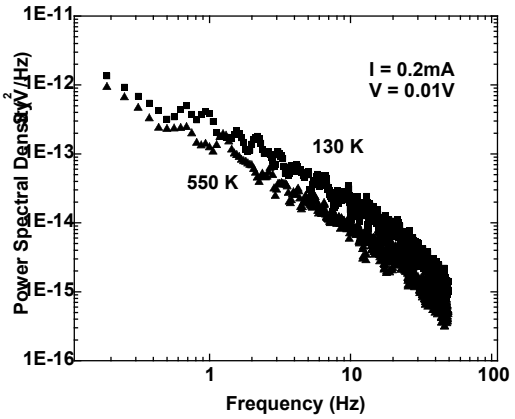

Fig. 6.1a: Power spectra densities of voltage fluctuations S_V for ELO-GaN at 550K. The S_v at 130K is included for comparison.

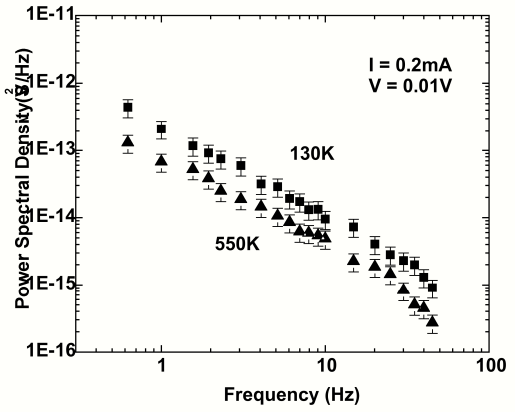

Fig. 6.1b: Power spectra densities of voltage fluctuations S_V, with error bars, for ELO-GaN at 550K. The S_v at 130K is included for comparison.

Table 6.1: Error bars of voltage power spectral density S_V at 550K for selected frequencies points.

Freq (Hz)	Ave S_V	Max S_V	Min S_V	Err (%)
6.25E-01	1.29E-13	1.33E-13	1.26E-13	2.84
1.00E+00	6.74E-14	7.62E-14	5.86E-14	13.07
1.56E+00	5.21E-14	5.50E-14	4.90E-14	5.72
1.94E+00	3.80E-14	3.93E-14	3.70E-14	3.06
2.31E+00	2.47E-14	2.80E-14	2.12E-14	13.5
3.06E+00	1.87E-14	2.00E-14	1.65E-14	8.86
4.06E+00	1.44E-14	1.50E-14	1.38E-14	4.39
5.13E+00	1.06E-14	1.15E-14	9.94E-15	7.46

6.06E+00	8.48E-15	8.79E-15	8.18E-15	3.47
7.00E+00	6.17E-15	6.35E-15	6.01E-15	2.83
7.94E+00	5.89E-15	6.51E-15	5.23E-15	10.8
9.06E+00	5.40E-15	5.82E-15	4.82E-15	8.98
1.00E+01	4.86E-15	5.01E-15	4.70E-15	3.05
1.49E+01	2.24E-15	2.47E-15	2.06E-15	9.26
2.01E+01	1.85E-15	1.97E-15	1.75E-15	5.96
2.50E+01	1.44E-15	1.67E-15	1.22E-15	15.5
3.01E+01	8.23E-16	8.81E-16	7.54E-16	7.20
3.51E+01	4.99E-16	5.51E-16	4.34E-16	11.5
4.00E+01	4.43E-16	4.94E-16	4.00E-16	10.9
4.51E+01	2.70E-16	3.09E-16	2.26E-16	15.0

At 550°C, the measured carrier concentration for ELO-GaN is 3.2×10^{16}cm^{-3} and carrier mobility is 132cm^2/Vs. The total carrier number within the 8μm thick bridge-shaped Hall-bar ELO-GaN is $N = 2.04\times10^8$. With a measured voltage of 0.01V, $\alpha \approx 0.66$ was obtained. The measurement errors of S_V at 550K for selected 20 frequency points within the range of 0.1-50Hz are shown in Table 6.1. The error is estimated to be about 10%.

Fig. 6.1 illustrates only the voltage power spectral densities S_V of ELO-GaN at 130K and 550K. For temperatures within this range, the noise parameters α were also evaluated and shown in Table 6.2. Note that the intercept points were taken with the gradient fixed at –1. These experimentally determined noise parameters α were also plotted against temperature variation as shown in Fig. 6.2 At high and low temperature ends, the noise parameter α tends towards higher values compared to α at room temperature. The possible explanation for this temperature-dependent behavior of α may be due to the possible increase of the piezopolaron coupling coefficient g. An investigation into this strain-dependent g will be carried out in the subsequent section.

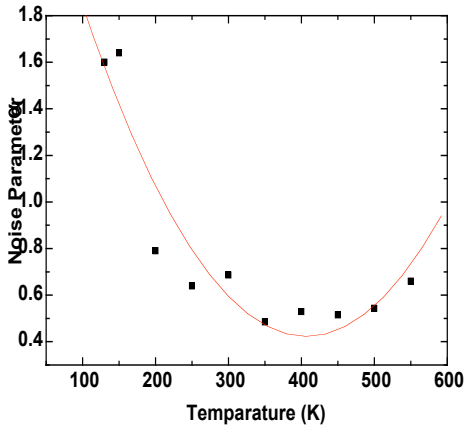

Fig. 6.2: Temperature dependence noise parameters α for ELO-GaN.

Table 6.2: Temperature dependence noise parameters α for ELO-GaN.

Temperature (K)	Intercept	α
130	-12.106	1.6
150	-12.094	1.64
200	-12.410	0.79
250	-12.504	0.639
300	-12.473	0.686
350	-12.624	0.485
400	-12.586	0.529
450	-12.598	0.515
500	-12.575	0.543
550	-12.490	0.66

6.2_Si-doped n-type GaN

Since dislocation rearrangement and other defects dominate in n^+-GaN:Si at high temperature, it will be more appropriate to evaluate the noise parameter α at room temperature in order to investigated the piezoelectric property. In this case, in addition to various scattering mechanisms, we expect that piezoelectric effect will play a comparative role and hence the appropriate estimation of the piezopolaron coupling coefficient g will be important (This issue will be addressed in the following section). The measured voltage power spectral densities S_V of n^+-GaN:Si are shown in Fig. 6.3 for a variety of operating voltages across the voltage terminals using a constant biasing current source. The spectra show $1/f$ behavior below 50 Hz.

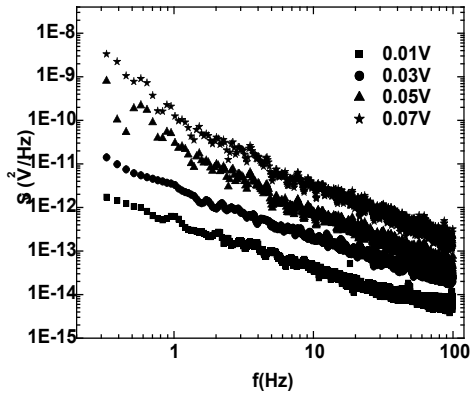

Fig. 6.3: Voltage power spectra densities S_V of n^+-GaN:Si for a variety of operating voltages.

At room temperature, the measured carrier concentration for n^+-GaN:Si is $6.94\times10^{17}cm^{-3}$ and carrier mobility is $100cm^2/Vs$. The total carrier number within the 2μm bridge-shaped Hall-bar n^+-GaN:Si is $N = 1.11\times10^9$. The 1 Hz $1/f$ noise levels of the bridge-shaped Hall-bar, plotted as a function of terminal voltage in Fig. 6.4, show a V^2 dependence for the terminal voltage below 0.07 V and the noise parameter at this range of terminal voltage is constant at $\alpha \sim 5$.

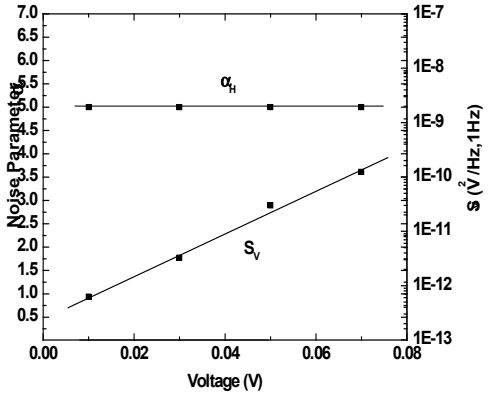

Fig. 6.4: Voltage dependence noise parameters α and voltage spectral densities S_V of n^+-GaN:Si at 1 Hz.

6.3 Results and Discussion

Studying quantum 1/*f* noise in semiconductors is important for understanding the physical processes that govern the transport of carriers [1]. There are different carrier-scattering processes possible, including *impurities scattering*, *polar* and *non-polar optical phonon scattering*, as well as *acoustic phonon scattering* [11]. In addition to impurities and electron-optical phonon scattering mechanisms, acoustic mode lattice scattering can also play an important role in determining 1/*f* noise in elemental semiconductors [1]. For ferroelectric materials, in particular, the interaction of electrons and transversal acoustic phonons has led to the discovery of piezoelectric scattering of carriers [12] and the development of theoretical explanations for *weak*, *intermediate* and *strong couplings* of piezoelectric polarons (conduction electrons coupled to acoustic phonons via the piezoelectric electron-phonon interaction) [13, 14].

6.4_The Energy-Momentum Relationship

The coupling theories revealed that the piezoelectric polaron obeys an anomalous energy-momentum $E(P)$ relationship. The curve starts out quadratic at small P but asymptotes to a straight line with slope equal to the speed of sound v_s at large P [15]. The physical picture proposed was that as the electron approaches the speed of sound, the electron-phonon interaction becomes strengthened because of the degeneracy. This causes an increasing number of acoustic phonons to take part in forming the lattice distortion around the electron. The large lattice distortion then traps the electron preventing it from traveling faster than the speed of sound [16]. In other words, for strongly piezoelectric crystals the coupling between elastic and electric variables has a profound influence on the nature of the acoustic modes and phonon transport. Through this coupling the material thus appears *elastically stiffened*, and the electron velocity and other characteristics of the wave are modified [17].

The $E(P)$ relationships derived from the coupling theories are summarized in Table 4.1 illustrating the *poloron self-energy* and *polaron mass*. In Table 4.1, $q_D = \omega_D/v_s$ is the Debye cut-off wave vector. The expression of piezopolaron self-energy has a complex form and for a detail derivation the readers are referred to reference [18].

The $E(P)$ relationship involves a dimensionless piezopolaron coupling coefficient g which is given as $g = e^2\left\langle e_{ijk}^2\right\rangle/\hbar\,\varepsilon_0^2\,cv_s$ where ε_0 and c are the static dielectric constant and the average elastic constant, respectively, and $\left\langle e_{ijk}^2\right\rangle$ is an average of the piezoelectric tensor components. The unit of wave vector used is $mv_s/\hbar$ and the unit of energy used is $m\,v_s^2$ where m is the conduction band mass and $\hbar = m = v_s = 1$. When g is much smaller than 1 ($g << 1$), it is generally agreed to use the weak coupling perturbation theory whereas when g is nearly equal to $3\pi/4$, the intermediate coupling theory is used. However, when g is nearly equal to $3\pi/4$, but much smaller than the cut-off phonon wave number q_D, i.e., ($3\pi/4 << g << q_D$), the strong coupling theory is employed [19].

Table 6.3: The energy-momentum $E(P)$ relationship for weak, intermediate and strong coupling theories.

Coupling Theories	The Ground-state Energy (meV)	The Polaron Mass
Weak [45]	$-\frac{4g}{\pi}\ln\left(\frac{q_D+2}{2}\right)$	$\frac{m}{m^*}=1-\frac{4g}{3\pi}$
Intermediate [45]	$-\frac{4g}{\pi}\ln\left(\frac{q_D+2}{2}\right)$	$\frac{m}{m^*}=\frac{1}{1+4g/3\pi}$
Strong [48]	$?-\frac{2g^2}{3\pi}$	$\frac{m}{m^*}=1+\frac{8g^2}{9\pi}$ $\frac{m}{m^*}=\frac{32}{27\sqrt{\pi}}g^2$

Notice that $\left\langle e_{ijk}^2\right\rangle/\varepsilon_0 c$ is the electromechanical coupling coefficient. For crystals having several independent piezoelectric tensor coefficients $\left\langle e_{ijk}^2\right\rangle$ there are numerous different electromechanical coupling coefficients that can be

defined, however, none of which solely provide a complete characterization of the influence of the *piezoelectric stiffening* [14]. For instance, if piezoelectricity is screen by any method, either totally or partially, the velocity of acoustic waves decreases. This can be done by the increase in their electrical conductivity, such as the case of heavily doped n-type gallium nitride (GaN), where the impurities absorb the electromagnetic radiation. It is desirable, therefore, to choose a suitable averaging of $\langle e_{ijk}^2 \rangle$ by which the strength of the piezoelectric coupling can roughly be gauged and the appropriate coupling theory (hence the appropriate energy-momentum relationship) be used.

6.5_Effect of Strain in GaN

The hexagonal GaN grown on sapphire (Al_2O_3) substrate crystallizes in the *wurtzite* structure belonging to the C_{6v}^4 ($C6_3mc$) space group. This class has piezoelectric and permittivity tensors which are invariant under rotations in the z-axis, therefore, it retains their *transverse-acoustic isotropy*. Typical GaN/Al_2O_3 heterostructure can exhibit strain/stress due to lattice mismatch and/or differences in their thermal expansion coefficients. The piezoelectric effect is present to a certain extent, due to the *strain-induced polarizations*. Depending on whether they are completely strained or completely relaxed at their growth temperature, defects such as misfit dislocations may be formed. Nevertheless, according to the *elastic continuum theory* [20], a defect will produce a strain field and if one of the constituent layers is of a piezoelectric material the misfit strain may produce strong piezoelectric fields, which are normal to the interface [21]. As a result, this has led us to focus our attention to internal strain and/or defect-induced strain with piezoelectric potential rather than to focus on the polaron interaction with dislocations and defects.

6.6_The Macroscopic Piezoelectric Equations

The *macroscopic piezoelectric equations* that relate the stress T_α, strain S_β, electric fields E_i and displacement field D_i are expressed as

$$T_\alpha = c_{\alpha\beta}S_\beta - e_{k\alpha}E_k \tag{23}$$

$$D_k = 4\pi e_{k\alpha}S_\alpha + \varepsilon_{ik}E_i \tag{24}$$

Note that repeated indices imply summation. The subscripts i, j, or k are (x,y,z) while α or β means xx, yy, zz, yz, xz, xy. The constant parameters are the familiar elastic constant $c_{\alpha\beta}$, the dielectric tensor ε_{ik}, and the piezoelectric constant $e_{k\alpha}$. Consider now the piezoelectric stiffening of the crystal, equation (23) can then be re-written as [14]

$$T_\alpha = \bar{c}_{\alpha\beta}S_\beta \tag{25}$$

where

$$\bar{c}_{\alpha\beta} = c_{\alpha\beta} + \frac{q_k e_{k\beta} q_i e_{i\alpha}}{q_m \varepsilon_{mn} q_n} \tag{26}$$

Notice the term $q_k e_{k\beta} q_i e_{i\alpha}/q_m \varepsilon_{mn} q_n c_{\alpha\beta}$, is actually the electromechanical coupling coefficient $\langle f \rangle$. Expression (26) shows that the piezoelectric interactions affect the elastic constants, and hence the speed of sound where $c = \rho v^2$. This in turn affects the piezopolaron coupling coefficient g, which is an important parameter for the determination of the noise parameter α to be discussed in the subsequent sections.

6.7_Piezopolaron Coupling Coefficient

Let us now consider more closely the dimensionless piezopolaron coupling coefficient g. For transversal acoustic phonon, we write the expression for g as [14]

$$g = \frac{e^2}{\hbar \varepsilon_0 \langle v_s \rangle} \langle f \rangle \tag{27}$$

As usual, we express $\langle f \rangle = q_k e_{k\beta} q_i e_{i\alpha}/q_m \varepsilon_{mn} q_n c_{\alpha\beta}$, which is the angular average electromechanical coupling coefficient in

the transversal acoustic mode. It is a measure of the strength of the electron-phonon coupling and it varies over direction of phonons, therefore its value is usually obtained by taking some average over different phonon directions.

Consider now the macroscopic piezoelectric equation given in (23), if there is no *tensile* or *compressive strain*, i.e., $S_\beta = 0$, which is a typical case for free-standing GaN epilayer such as ELO-GaN, then the built-in stress will be $T_\alpha = - e_{k\alpha}E_k$. Here the electric field E_k is expressed as $E_k = 2e_{k\alpha}\Delta\varepsilon/\varepsilon_0\varepsilon$, where $\Delta\varepsilon = \varepsilon_{\parallel} - \varepsilon_{\perp}$, is the *tetragonal distortion* of the piezoelectric layer [52]. Note that E_k is an average value and the averaging has been made by the angular average of the piezoelectric coupling constants $e_{k\alpha}$ written as [7],

$$\left\langle e_{ijk}^2 \right\rangle = \frac{2}{35}\left(e_{33} - e_{31} - e_{15}\right)^2 + \frac{16}{105}e_{15}\left(e_{33} - e_{31} - e_{15}\right) + \frac{16}{35}e_{15}^2 \tag{28}$$

Wurtzite-structure GaN has three independent piezoelectric constants, e_{15}, e_{31}, and e_{33} with respective values of -0.30Cm^{-2}, -0.33Cm^{-2} and 0.65Cm^{-2} [54]. The dielectric tensors are $\varepsilon_{11} = \varepsilon_{\perp} = 8.6$ and $\varepsilon_{33} = \varepsilon_{\parallel} = 10.1$ [55]. Therefore, E_k can be estimated to be $E_k = 6.281\times10^9$ V/m. Since we are concerned only with the shear mode along the *c* axis, the built-in shear stress can be evaluated as $T_{xx} = T_{yy} = 1.88$ GPa. This is a theoretical calculated shear stress, in a typical GaN epilayer, however, the built-in shear stress is in the order of < 1.5 GPa [56]. The possible explanation for the difference between the theoretical and experimental shear stresses may be due to the formation of misfit dislocations, hence, typical GaN epilayer exhibits lower shear stress compared to the calculated value.

The piezoelectrically stiffened transversal acoustic phonon velocity is expressed as $v_s = \sqrt{c_{ii}\left(1 + k^2\right)\rho}$ [57]. Here, c_{ii} is the elastic modulus relevant for the bulk acoustic-wave, $\rho = 6150$ kg/m^3 is the mass density of GaN [54] and $k^2 = \left\langle f \right\rangle$ is the electromechanical coupling coefficient, which leads to piezoelectrically stiffened elastic constants if displacement along the *c* axis is involved in the wave propagation. For shear mode, $k^2 = e_{15}^2/\varepsilon_0\varepsilon_{11}c_{44}$. Substituting for k^2, $v_s = \sqrt{\left(c_{44} + e_{15}^2/\varepsilon_0\varepsilon_{11}\right)\rho}$. In order to obtain a shear strain dependent transversal acoustic phonon velocity, we need to express c_{44} as $(T_{11}+e_{15}E_k)/S_{11}$ from equation (4.1). Therefore, we obtain

$$v_s = \sqrt{\left[\left(T_{11} + e_{15}E_k\right)/S_{11} + e_{15}^2/\varepsilon_0\varepsilon_{11}\right]\rho} \tag{29}$$

Note that the second term of the above expression contributes less significantly to the transversal acoustic phonon velocity v_s, therefore, it is sufficient that only average values for the piezoelectric coupling constant $\left\langle e_{ijk}^2 \right\rangle$ and static dielectric constant ε_{11} will be used. The assumptions made here, however, are that the electric field $E_k = 6.281\times10^9$ V/m as well as the built-in shear stress $T_{11} = 1.88$ GPa are not changing with the shear strain. These assumptions are made in the belief that for any increment of shear strain, the changes in the shear stress T_{11} and electric field E_k will be accommodated by the formation of misfit dislocations. However, the point worth mentioning here is that there is a singularity occurring at $S_{11} = 0$. As a result, we need to limit the S_{11} value to -1×10^{-6}. The negative sign indicates compressive strain. Fig. 6.5 shows a theoretical evaluated shear strain dependent transversal acoustic phonon velocity. The plot reveals that the velocity approaches a high value of about 7×10^3 m/s at $S_{11} = -1\times10^{-6}$. As the shear strain increases, i.e., it becomes more compressive, the velocity decreases to a constant minimum value of about 1×10^3 m/s at a strain value of around -1×10^{-5}.

Consider now the electromechanical coupling coefficient $\left\langle f \right\rangle = q_k e_{k\beta} q_i e_{i\alpha}/q_m\varepsilon_{mn}q_n c_{\alpha\beta}$. For transversal acoustic phonon, $\left\langle f \right\rangle$ can be expressed as $\left\langle f \right\rangle = k^2 = e_{15}^2/\varepsilon_0\varepsilon_{11}c_{44} = e_{15}^2/\rho\varepsilon_0\varepsilon_{11}v_s^2$ where $c_{44} = \rho v_s^2$. Since v_s is strain dependent as expressed in (4.7), this implies that $\left\langle f \right\rangle$ is also strain dependent. Nevertheless, similar to the situation of the electric field E_k and shear stress T_{11}, we have chosen to fix the electromechanical coupling coefficient $\left\langle f \right\rangle$ at zero shear strain and observe the strain dependent piezopolaron coupling coefficient *g*. From expression (4.5), a strain dependent *g* is plotted as shown in Fig. 4.1. It shows that *g* varies approximately from 1.36 at $S_{11} = -1\times10^{-6}$ to 8.85 at $S_{11} = -5\times10^{-5}$.

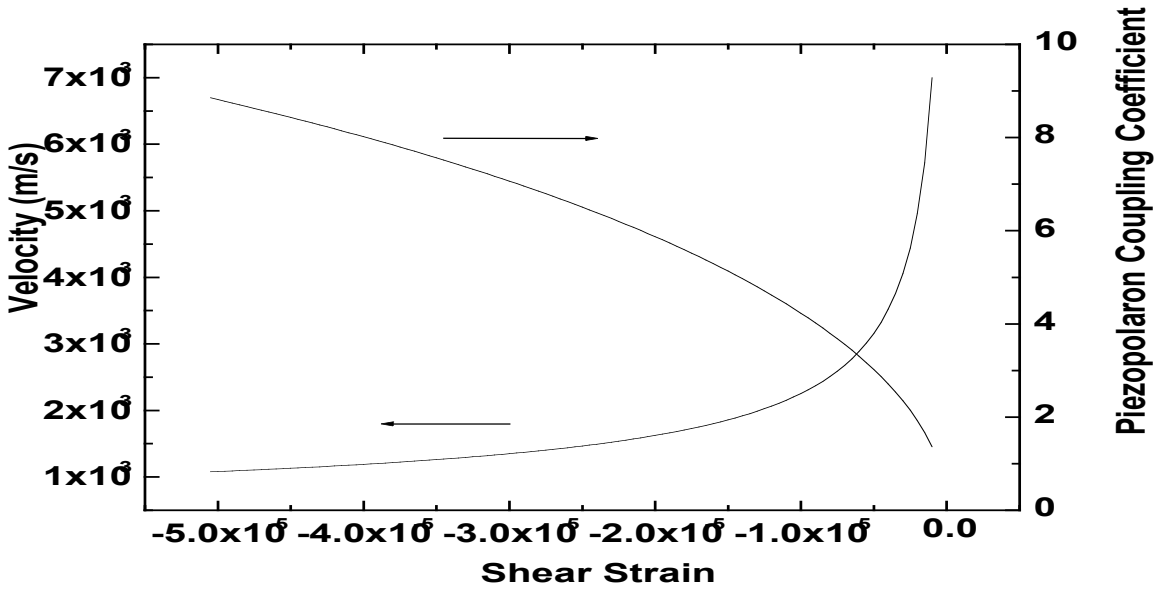

Fig. 6.5: Strain dependence of velocity of transversal acoustic phonon v_s and piezopolaron coupling coefficient g.

6.8_Low Frequency Noise in Epitaxial Lateral Overgrown GaN

In our ELO GaN, we evaluated the shear strain S_{11} by measuring the frequency shift of the high frequency E_2(TO) phonon utilizing Raman spectroscopy. The strain tensor components are given as $S_{11} = S_{22} = \Delta\omega_\lambda/(2a_\lambda+b_\lambda q)$ and $S_{33} = qS_{11}$. Here, λ is the E_2(TO)(High) phonon mode, $\Delta\omega$ is the change of frequency, a and b are the phonon deformation potential constants and $q = -2c_{13}/c_{33}$. In our ELO-GaN, the measured change of E_2(TO)(High) phonon frequency $\Delta\omega_{E2}$ was negligible. With $a = -850\text{cm}^{-1}$ and $b = -920\text{cm}^{-1}$ and using $c_{13} = 106$ GPa and $c_{33} = 398$ GPa, we estimated the shear strain tensors $S_{11} = S_{22} = -5\times10^{-6}$. This corresponds to a piezopolaron coupling coefficient of $g = 3$.

At low electric field the drift velocity u is proportional to the electric field strength E, i.e., $u = \mu E$. For our ELO-GaN, the measured mobility was $\mu = 132\text{cm}^2/\text{Vs}$ at 550K. With an applied voltage of 0.01V, the electric field evaluated was $E = 0.625$V/cm, this corresponds to $u = 82.5$cm/s. Since u is very much smaller than v_s, we employed the expression $s' = 2gN'\hbar/3\pi m^* v_s$ from section 2.6 to evaluate s'. With $N' \sim 10^8$ carriers/cm length for ELO-GaN, s' evaluated is about 1000. Since s' is large, it is sufficient to use coherent piezoelectric quantum $1/f$ noise theory. Indeed, the large s' causes the weight $1/(1+s')$ of the conventional quantum $1/f$ term to be comparatively small, and the weight of the coherent term to be almost unity. As a result, the quantum $1/f$ coefficient α is simplified to $\alpha = 2g/\pi$ which yields 2 for $g = 3$. This result correlates well with our experimentally obtained α which has values within the range 0.5-2.

Note that slight non-uniformities present in any sample could slightly increase the theoretical α value above 2. They could also down-correct the measured α to values below 0.5, because the assumed number of carriers in the expression $\alpha = S_I f N/V^2$ used by us to define the measured α may have been slightly larger than the effective number that remains when non-uniformities are taken into account.

6.9 Low Frequency Noise in n^+-GaN:Si

For our n^+-GaN:Si sample, the measured change of E_2(TO)(High) phonon frequency was $\Delta\omega_{E2} = 0.6\text{cm}^{-1}$. The estimated shear strain tensors were $S_{11} = S_{22} = -1\text{-}3\times10^{-5}$. The measured carrier mobility for our n^+-GaN:Si sample was $\mu = 100\text{cm}^2/\text{Vs}$ at room temperature. With an applied voltage of $V < 0.1$V, the electric field $E = 6.25$V/cm, this corresponds to $u = 625$cm/s. Similar to the case of ELO-GaN, with u small compared to v_s and since N'

~ 10^9 carriers/cm length for n^+-GaN:Si, it is sufficient to use the coherent piezoelectric quantum 1/*f* noise theory. As a result, the estimated quantum 1/*f* coefficient α was 4-7. This result correlates well with our experimentally obtained α value, which is 5.

8. CONCLUSIONS

The theoretical values of the noise parameter α for both ELO-GaN and Si doped n^+-GaN:Si/Al_2O_3 epilayers were estimated with the strain dependence dimensionless piezopolaron coupling coefficient *g* based on the strain dependence transversal acoustic phonon velocity. The experimentally obtained α for both ELO-GaN and n^+-GaN:Si samples correlate well with the theoretically estimated α. The energy-momentum $E(P)$ relationships given in Table 4.1 allows us to estimate the polaron self-energy as well as the polaron mass. Since the piezopolaron coupling coefficients *g* for both ELO-GaN and n^+-GaN:Si are greater than $3\pi/4$, the strong coupling theory will be appropriate here. For ELO-GaN, the polaron self-energy estimated was -1.91meV and the polaron mass was m* = 0.282m. Since the estimated polaron mass is heavier than the effective electron mass which is given as m* = 0.2m [54], the estimation of the strain dependence piezopolaron coupling coefficient for ELO-GaN is justifiable. In conclusion, the theoretically estimated noise parameter α based on coherent piezoelectric quantum 1/*f* noise agrees with the experimentally obtained results for ELO-GaN. This result indicates that piezoelectric effect is indeed relevant both for the transport process in ELO-GaN and for its fluctuations.

For lattice-dynamical (piezoelectric Q1/f noise based on TA infraquanta) the weight parameter, or coherence parameter, s' has the same role as the parameter s had for the usual (QED) Q1/f noise. It gives a rough interpolation approximation of the piezoelectric Q1/f coefficient by combining the conventional and coherent parts in a weighted sum

$$\alpha_H = fNS_{\delta j/j}(f) = [1/(1+s')](4g/3\pi)(\Delta\mathbf{k}/k_s)^2 + [s'/(1+s')]\{2g/\pi[1-(\langle\mathbf{k}\rangle/k_s)^2]\}, \quad (30)$$

where v_s is the speed of sound, $\langle\mathbf{k}\rangle = m^*\langle\mathbf{v}\rangle/\hbar$, $|\langle\mathbf{v}\rangle| = u$ is the drift velocity of the carriers, $\Delta\mathbf{k}/k_s = \Delta\mathbf{v}/v_s$, and

$$k_s = m^*v_s/\hbar; \quad s' = (gN'\hbar/\pi m^*v_s)(v_s/u)^3F(u/v_s). \quad (31)$$

Here N' is the number of carriers per unit length of the sample in the direction of current flow, and

$$F(u/v_s) = 2(u/v_s)\{1 + 1/[1 - (u/v_s)^2]\} + \ln[1-(u/v_s)]^2 - \ln[1+(u/v_s)]^2. \quad (32)$$

The coherence parameter s' was calculated in the same way in which s was introduced in the QED case for the connection between coherent and conventional Q1/f). It is the ratio of the coherent piezoelectric energy of the drift motion divided by the additional kinetic energy of the carriers introduced by the drift velocity u.

Acknowledgements. This work was supported by ONR, AFOSR, (MURI 17/2001), by the Agency for Science, Technology and Research (A*STAR) and Fujitsu Quantum Devices Singapore (FQDS).

References

1. P.H. Handel: "Noise, Low Frequency", Wiley Encyclopedia of Electrical and Electronics Engineering, vol. 14, pp. 428-449, John Wiley & Sons, Inc., 1999.
2. P.H. Handel: "Noise" in *Survey of Semiconductor Physics* (K.W. Böer Editor) IInd Edition, Vol.2, J. Wiley & Sons 2002, pp. 203-219.
3. P.H. Handel: "Coherent States Quantum 1/f Noise and the Quantum 1/f Effect", in *Noise in Physical Systems and 1/fNoise*, N. Holland Publ. Co. 1985, pp. 465-468.
4. P.H. Handel and T.Musha: "Coherent Quantum 1/f Noise from Electron-Phonon Interactions", Zeitschrift für Physik B 70, 515-516 (1988).
5. P.H. Handel and A.G. Tournier, "Nanoscale Engineering for Reducing Phase Noise in Electronic Devices," Proc. IEEE 93, 1784-1814 (2005).
6. H. Tang, W. Kim, A. Botchkarev, G. Popovici, F. Hamdani and H. Morkoc, *Solid-State Electronics*, **42**, 839, 1998.
7. G. Bertotti, A. Ferro, F. Fiorillo and P. Mazzetti, *Dislocations in Solids*, **7**, 1, 1986.
8. K. Hiramatsu, T. Detchprohm and I. Akasaki, I., *Jpn. J. Appl. Phys*., **32**, 1528, 1993.
9. K. Kim, W. R. Lambrecht and B. Segall, *Phys. Rev. B*., **53**, 16310, 1996.
10. F. N. Hooge, *IEEE TED*, **41**, 1926, 1994.

11. G. S. Kousik, C. M. van Vliet, G. Bosman and P. H. Handel, *Adv. Phys*., **34**, 663, 1986.
12. A. R. Hutson, *J. Appl. Phys*., **32**, 2287, 1961.
13. C. B. Duke and G. D. Mahan, *Phys. Rev*., **139**, A1965, 1965.
14. G. D. Mahan, *Polarons in Ionic Crystals and Polar Semiconductors*, edited by J. T. Devreese, North-Holland, Amsterdam, 553, 1972.
15. G. Whitfield and I. Gerstner, *Phys. Rev*., **165**, 993, 1968.
16. J. Thomchick and G. Whitfield, *Phys. Rev. B*, **9**, 1506, 1974; **10**, 3458, 1974.
17. B. A. Auld, "Acoustic Fields and Waves in Solids," *R. E. Kriger Publishing Company*, Malabar, FL, vol. II, 1990.
18. T. Holstein, *Anns. Phys*., **29**, 410, 1964; G. D. Mahan and C. B. Duke, *Phys. Rev*. **149**, 705, 1966; L. Hedin and L. Lundqvist, in *Solid State Physics: Advances in Research and Applications*, edited by F. Seitz, D. Turnbull and H. Ehrenreich, **23**, 1, 1969.
19. K. Okamoto, *J. Phys. Soc. Jpn*., **32**, 46, 1972; **36**, 62, 1974.
20. L. D. Landau and E. M. Lifshitz, *Theory of Elasticity*, Pergaon, 1959.
21. E. Anastassakis, *Solid State Comms*., **84**, 47, 1992.